Supporting Information

A pH-dependent conformational switch controls *N. meningitidis* ClpP protease function

Zev A. Ripstein[1,2†*], Siavash Vahidi[1,2,3,4†‡*], John L. Rubinstein[1,2,5*], Lewis E. Kay[1,2,3,4*]

[†] These authors have contributed equally

[1]Department of Biochemistry, University of Toronto, Toronto, Ontario, M5S 1A8, Canada

[2]Program in Molecular Medicine, Hospital for Sick Children, Toronto, Ontario, M5G 1X8, Canada

[3]Department of Molecular Genetics, University of Toronto, Toronto, Ontario, M5S 1A8, Canada

[4]Department of Chemistry, University of Toronto, Toronto, Ontario, M5S 1A8, Canada

[5]Department of Medical Biophysics, University of Toronto, Toronto, Ontario, M5G 1L7, Canada

[‡]Present address: Department of Molecular and Cellular Biology, University of Guelph, Guelph, Ontario, N1G 2W1, Canada

*Correspondence to: zevripstein@gmail.com; svahidi@uoguelph.ca; kay@pound.med.utoronto.ca; john.rubinstein@utoronto.ca

Materials and Methods

Plasmids, constructs, protein expression and purification The *clpP* (Uniprot: Q9JZ38) and *clpX* (Uniprot: Q9JYY3) genes from *Neisseria meningitidis* were obtained, cloned, and the corresponding proteins recombinantly expressed and purified as described previously.[1] Transformed BL21(DE3) *E. coli* cells were grown in minimal M9 $^{2}H_2O$ media for all NMR measurements and degradation assays, and in LB media for cryo-EM analysis. Protein concentrations were determined spectrophotometrically (GdnCl-denatured protein) using extinction coefficients obtained from ExPASy's ProtParam web-based tool (https://web.expasy.org/protparam/).

MMTS labeling Purified I144C NmClpP, labeled as [U-^{2}H; Ileδ1-$^{13}CH_3$; Leu/Val-$^{13}CH_3/^{12}CD_3$; Met-$^{13}CH_3$] (referred to as "ILVM labeling", and prepared as described previously[2]) was incubated with 5 mM DTT for 1 hour. DDT was removed by buffer exchange with a degassed 100 mM KCl, 50 mM Tris pH 8.5 solution using an Amicon Ultra-15 50K MWCO (Millipore) concentrator. A DMSO stock solution of 100 mM ^{13}C-methyl-methanethiosulfonate (^{13}C-MMTS; Isotec) was added in 20% molar excess to a solution of the protein (total volume ~2.5 mL) and allowed to react overnight at room temperature. The reactions were terminated by buffer exchange into 50 mM imidazole, 100 mM KCl, pH 7.0 prepared in 100% $^{2}H_2O$. The two natively occurring Cys residues in NmClpP are buried and therefore unreactive towards MMTS. The MMTS labeling approach is necessary here because ^{1}H-^{13}C correlation maps of ILVM-labeled NmClpP are, in general, of poor quality and highly overlapped. Comparison of well-resolved ILV ^{1}H-^{13}C resonances of MTC-labeled and wild-type NmClpP establish that the introduction of ^{13}C-MTC to NmClpP does not lead to structural perturbations (Figure S2). While

this construct has lower activity than the wild-type enzyme, possibly due to a perturbed catalytic region, its activity responds similarly to pH changes (Figure S5).

NMR Spectroscopy HMQC-based ^{1}H-^{13}C correlation spectra exploiting a methyl-TROSY effect specifically developed for applications to high molecular weight proteins[3] were recorded at 18.8 T and 40 °C using a Bruker AVANCE III HD spectrometer equipped with a cryogenically cooled xyz pulsed-field gradient triple-resonance probe. Spectra were processed using the *NMRPipe* suite of programs,[4] analyzed using scripts written in-house, and visualized using *Ccpnmr*.[5] For both NMR measurements and degradation assays, the samples were buffer exchanged into a mixture of buffering reagents (monosodium citrate, dipotassium phosphate, Tris and Caps each at 10 mM) prepared in 99.9% $^{2}H_2O$. pH values were measured at room temperature and corrected for the isotope effect. Samples were adjusted to pH 5.0 at the onset of the titration with $NaO^{2}H$ and subsequently adjusted during the course of the titration by the addition of small volumes of concentrated ^{2}HCl.

Rationale for employing MMTS labeling to study NmClpP

The ClpP protease is a structurally heterogenous and highly dynamic molecule[6–11]. In NMR spectra this manifests in multiple peaks for a single site and often very significant line broadening. For example, in a previous study of *S. aureus* ClpP we assigned seven peaks in the ^{1}H-^{13}C HMQC correlation map to the Ile8-δ1 methyl group in the N-terminal domain and three peaks to Ile138-δ1 in the handle region.[7] In a separate study, severe line broadening and peak overlap precluded the assignment of ILVM methyl groups of *M. tuberculosis* ClpP2, although, interestingly, we were able to assign the great majority of correlations in spectra of *M.*

tuberculosis ClpP1.[12] Similarly, the ^{1}H-^{13}C HMQC spectra of ILVM-labeled NmClpP in the present study are of low quality with overlapped and broad peaks.

Initial attempts to follow intensity- and peak position-changes as a function of pH for well-isolated ILVM resonances with high signal-to-noise ratios in NmClpP, a total of 69 peaks, was not informative. Fifty three such correlations do not titrate with pH (examples are shown Figure S3), while sixteen resonances undergo changes in intensity as a function of pH (examples are shown Figure S4) that do not appear to reflect the structural changes observed in our cryo-EM structures (Figure 2C and 2D) and that cannot be used to explain our functional assays (Figure 2B - green). Notably, for these correlations intensity changes were small and in no case did peak intensities decrease to zero at high pH or increase from zero (low pH) and plateau at high pH values, as would be expected for probes of a significant conformational change over this pH range. This is perhaps not surprising. On the basis of the known structural changes to NmClpP, reported here, one would expect only four methyl-containing residues (Ile144, Ile142, Leu135, and Ile131, all in the handle region) to report on the extended ⇌ compressed equilibrium. However, it is likely these residues are overlapped or exchange-broadened so that they cannot be used for analysis. With this in mind, we opted to pursue an MMTS-labeling strategy, which offers the following advantages:

1) MMTS labeling provides a facile means for the introduction of a $^{13}CH_3$ group at a reactive Cys position to form a ^{13}C-MTC residue that can be used as a highly specific probe of protein structure, binding, and/or dynamics in supramolecular systems.[13] Cross-peaks from ^{13}C-MTC methyl-groups are localized to a region in the ^{1}H-^{13}C HMQC spectrum that is unobstructed from other protein resonances. As such, conformational transitions can be monitored free from interference of unwanted peaks, as demonstrated in studies of the proteasome,[13] the ClpP

protease,[7,13] and the AAA+ VAT translocase.[14] In cases where ILVM methyl spectra are overlapped, and a very specific question is considered, the advantages of the specific labeling approach are clear.

2) In studies of proteins where structural dynamics are to be probed over the complete molecule the ILVM-labeling approach is powerful. However, this does require that assignment of methyl groups to specific sites must first be achieved. In contrast, in cases where a very specific question is to be addressed it is often simpler and considerably faster to place a methyl group close to the site of interest, and use it as a 'focussed' probe, providing the information of interest. In this situation the assignment 'problem' is eliminated. In the present study where only the handle region undergoes a significant conformational change (see main text and Figure S11) the judicious placement of a methyl probe has proven to be critical.

3) As described above, a difficulty in studies of many different ClpPs arises from pervasive conformational heterogeneity. In general, methyl probes are less sensitive to the effects of conformational exchange than backbone amides and of all methyl groups, those from Met are very often the least affected from μs-ms timescale motions. As such, the MTC residue (effectively a Met with S replaced by C) is an excellent choice.

MMTS label only minimally perturbs the structure of NmClpP

As with the introduction of any label, care must be taken to ensure that structural changes are minimal. Although the MMTS label does result in changes to the ^{1}H-^{13}C HMQC spectrum of NmClpP, these are small (Figure S2A). Figure S2B quantifies the chemical shift perturbations (CSPs) that were observed using the method of Farmer et al.[15] in which the minimum chemical shift perturbation in response to the addition of label is calculated. This approach is useful in

cases where assignments of the unlabeled (non-MMTS) and labeled protein are not available, as is the situation here. For the majority of resonances in NmClpP the correspondence between peaks in unlabeled and labeled protein is clear, as correlations superimpose. In cases where this is not the case a minimum CSP is calculated as the distance between a peak in one spectrum and the closest peak in the second. As Figure S2B highlights, CSPs no larger than 0.2 ppm are calculated, with a median of 0.034 ppm. Such small changes are typical for amino acid substitutions that do not perturb the overall structure of the protein. As a second control we have compared the peptidase activities of wild-type and ^{13}C-MTC144 NmClpP as a function of pH (Figure S5), showing the same apparent pK_a value, a result consistent with little change in structure. The reduced activity noted likely reflects subtle structural changes (sub-Å), however, that can have large effects on catalysis.

In order to explore structural perturbations further we have obtain a low-resolution cryo-EM structure of MTC144 NmClpP, pH 8.5 (Figure S2C, described in more detail below) and compared the resulting conformation to those obtained of unlabeled NmClpP at pH 7.0 (compressed, inactive) and pH 8.5 (extended, active). The structure of MTC144 NmClpP clearly shows that it is in the extended, active form, with a well defined handle region, as expected given the high pH used, with a much better fit to the extended conformer density than to that from the compressed form (Figure S2C, and see below). Taken together, the CSP data, the functional assays, and the structure of MTC144 NmClpP establish that the addition of MMTS label results in only very small changes in structure, with the high pH form retaining the extended, active conformation.

Peptidase rate measurements Peptidase activities were measured at 40 ˚C with 1 μM ^{13}C-MTC144 NmClpP (monomer) and 250 μM PKM-AMC (acetyl-L-Pro-L-Lys-L-Met-7-amino-4-methylcoumarin group) used as substrate. This short peptide substrate was chosen because its small size allows it to diffuse freely into the degradation chamber of NmClpP regardless of the status of the axial pores. The reaction was monitored using a Synergy Neo2 96-well microplate reader by taking a measurement every 21 seconds for 60 minutes at λ_{ex}: 355 nm, λ_{em}: 460 nm. All functional assays were performed using deuterated enzyme in 100% $^{2}H_2O$-based NMR buffer to ensure maximum similarity with the NMR pH titrations. Activities are derived from initial rates extracted and analyzed using a Python script written in-house. Error bars correspond to one standard deviation derived from three repeat measurements.

Fitting of NMR data and activity assays To obtain the acid equilibrium constant for the ionization of His145 corresponding to

$$His^{H+} \leftrightharpoons H^+ + His$$

a 50 μM (monomer) sample of ^{13}C-MTC144 NmClpP was titrated over a pH range extending from 5 to 10. The decrease in the normalized peak volume of the peak corresponding to His^{H+} ($V_{His^{H+}}$= $V_{His^{H+}}$(pH)/ $V_{His^{H+}}$(pH=5.0)) and the concomitant increase in the normalized peak volume of *His* (V_{His}=V_{His}(pH)/V_{His}(pH=9.6)) were quantified using the *NMRPipe* suite of programs.[4] The changes in normalized peak volumes can be modelled using a simplified Henderson-Hasselbalch equation assuming a single pK_a

$$V_{His^{H+}} = \frac{1}{1 + 10^{pH - pK_a}}$$

$$V_{His} = 1 - \frac{1}{1 + 10^{pH - pK_a}}$$

where V_{His} and $V_{His^{H+}}$ are the fractional populations of *His* (Figure 2B – red circles) and His^{H+} (Figure 2B – blue circles), as established from ^{1}H-^{13}C HMQC correlation maps (Figure 2A). Activity profiles of ^{13}C-MTC144 NmClpP were measured from initial velocities of PKM-AMC substrate hydrolysis as a function of pH (Figure 2B – green circles). Activity is defined as

$$Activity = V_{His} \times V_0$$

where V_0 is a proportionality constant that converts the fractional population of the active *His* species, V_{His}, to activity. The NMR (two curves) and activity data (a single curve) were fit simultaneously to their respective equations indicated above. This was achieved using a least squares in-house script that takes advantage of a Levenberg-Marquardt search engine available within the lmfit (v. 0.9.14) package[16] in Python 3.8. Errors in the fitted parameters, pK_a and V_0, were estimated using a 10,000 repeat Monte Carlo simulation,[17] described in detailed previously.[8] The values obtained from Monte Carlo repeats were converted to a histogram, which was subsequently fit to a normal distribution function to yield expectation values and standard deviations σ. Final errors are reported as 2σ in the extracted values (95% confidence interval).

More complicated and likely more realistic models can be fit to our data. An obvious model explicitly takes into account the inactive ⇌ active equilibrium, and the protonation-deprotonation of His145 in both states (i.e., two pK_a values). However, the additional parameters that are required in such a model are highly correlated, and thus no further insight is obtained than from the simple model used here. It is important to understand, however, that the pK_a fitted by the simple model is an apparent value.

Preparation of Samples for Cryo-EM The NmClpXP complex was prepared as described previously,[1] and adjusted to pH 7.0. Briefly, 140 μM NmClpP (monomer concentration) was incubated with 120 μM NmClpX for 5 minutes before application onto a Superdex 200 Increase 10/300 (GE) gel filtration column equilibrated with 100 mM KCl, 50 mM Imidazole, 2 mM MgATP, pH 7.0 as the running buffer. Fractions corresponding to the doubly capped ClpXP peak were collected, placed on ice and vitrified within 10 minutes of elution.

Cryo-EM samples of NmClpP in isolation at pH 7.0 and at pH 8.5 were prepared by applying purified NmClpP onto a Superdex 200 Increase 10/300 (GE) gel filtration column equilibrated with either 100 mM KCl, 50 mM Imidazole, pH 7.0, or 100 mM KCl, 50 mM bicine, pH 8.5, as the running buffer. Peaks corresponding to the tetradecamer were pooled and concentrated to ~20 mg/mL. IGEPAL CA-630 (Sigma-Aldrich) was added to a final concentration of 0.025% before vitrification to increase the proportion of protein complexes adopting side views on the grid.

All samples were vitrified with a modified FEI Vitrobot mark III at 4 °C and ~100% relative humidity. 2.5 μL of sample mixtures were applied to nanofabricated holey gold grids[18] with a hole size ~1-2 μm, before plunge freezing into a 60:40 propane:ethane mixture held at liquid nitrogen temperature.[19] For the ClpXP complex at pH 7.0, grids were glow discharged in air for 15 seconds, and blotted for 15 seconds. For ClpP alone no glow discharge was used, and grids were blotted for 4.5 seconds.

Electron Microscopy NmClpXP at pH 7.0 was imaged with a Thermo Fisher Scientific Titan Krios G3 microscope operating at 300 kV and equipped with a Falcon III direct electron detector. Counting mode movies consisting of 30 frames obtained over a 60 second exposure

were collected with defocuses ranging from 0.5 to 2.0 μm. Movies were collected at a nominal magnification of 75,000×, corresponding to a calibrated pixel size of 1.06, with an exposure rate of 0.8 electrons/pixel/s and a total exposure of ~43 electrons/Å^2. A total of 3,594 movies was collected using *EPU* software.

The ClpP alone structures at pH 7.0 and pH 8.5 were calculated from images taken with a FEI Tecnai F20 microscope operating at 200 kV and equipped with a Gatan K2 Summit direct electron detector. Counting movies consisting of 30 frames obtained over a 30 second exposure were obtained with defocuses ranging from 0.5 to 3.0 μm. Movies were collected in counting mode at a nominal magnification of 25,000× corresponding to a calibrated pixel size of 1.45 Å with an exposure rate of 5 electrons/pixel/s and a total exposure of ~35 electrons/Å^2.

EM image analysis For the NmClpXP at pH 7.0, dataset movies were aligned and averaged using patch-based alignment implemented in *cryoSPARC* v2[20] with a 10×10 grid. Patch based CTF determination was then carried out on the resulting micrographs, and particles images were manually picked to generate 2D class averages that were then used as templates for particle selection. Particle images were extracted in 256×256-pixel boxes for further analysis. 2D classification was performed in three batches, and particle images belonging to classes corresponding to ClpXP complexes were selected and carried forward. Ab initio structure determination and classification was performed in *cryoSPARC* v2, and the class corresponding to a full ClpXP complex was used as a starting point in two successive rounds of heterogenous classification runs with D7 symmetry and 4 classes. The 742,377 particle images assigned to the dominant class were then refined with D7 symmetry yielding a map at 3.2 Å resolution of the ClpXP complex with weak and fragmented density for the bound ClpX due to incoherent

averaging, but excellent density for the ClpP portion. A slightly preferred orientation in the Euler angle distribution for particle images led to decreased resolution in the direction along the symmetry axis of the complex (Figure S7) but which was of sufficient quality to build an atomic model. Reconstructions with C1 symmetry showed a strong preferred orientation of the ClpX portion of the map, however the ~15° angle[1] between ClpX and ClpP resulted in a final reconstruction with limited differences in directional FSCs and a calculated sphericity of 0.89, with limited artifacts in the map.[21]

Movies of NmClpP alone (pH 8.5) were aligned and averaged using whole frame alignment implemented in *cryoSPARC* v2. CTF estimation and template picking was followed by individual particle local motion correction and extraction in 160×160-pixel boxes. Following 2D classification, and multiple rounds of heterogeneous classification 50,403 particle images were used for a final refinement with D7 symmetry, achieving a resolution of 4.1 Å (Figure S9). Further classification without applying symmetry did not yield additional conformations. To obtain the structure of the inactive form, a solution of NmClpP was adjusted to pH 7.0 and was subjected to the same cryo-EM analysis as described above resulting in 68,731 particle images input into a final refinement using D7 symmetry. This approach led to a map at a resolution of 4.4 Å. The map showed the same handle helix unwinding and compression as in the ClpXP map.

Atomic Model Building and Refinement To model ClpP bound to ClpX at pH 7.0, a single ClpP chain of the previously solved NmClpXP complex (PDB 6VFX[1]) was rigid body fit into the density using *UCSF Chimera,*[22] followed by manual adjustment to fit the density map in *Coot.*[23] The monomeric structure was then refined using D7 symmetry in *Rosetta*[24] to generate 100 models, the high scoring models were visually inspected and final modifications were made in

Coot, before further relaxation. Models were evaluated with *PHENIX*[25] to generate validation reports using *phenix.validation_cryo-EM* and *EMRinger*.[26] Figures of maps and models were generated in *UCSF Chimera* and *UCFS ChimeraX*.[27]

Cryo-EM structural analysis of MTC144 NmClpP

A 7.5Å map of ^{13}C-MTC144 NmClpP (pH 8.5) was obtained in the same manner as detailed above for NmClpP pH 8.5. Briefly 206 micrographs were collected resulting in 31,723 particle images, which after repeated 3D classification yielded 6,743 particles used in the final refinement. The map clearly shows ClpP in the active extended conformation (Figure S2C), consistent with the proper formation of the handle region**.**

Data Deposition Cryo-EM density maps and models have been deposited in the EMDB with accession numbers EMD-23000, EMD-23001, and the PDB with accession number 7KR2.

Supplementary Figures:

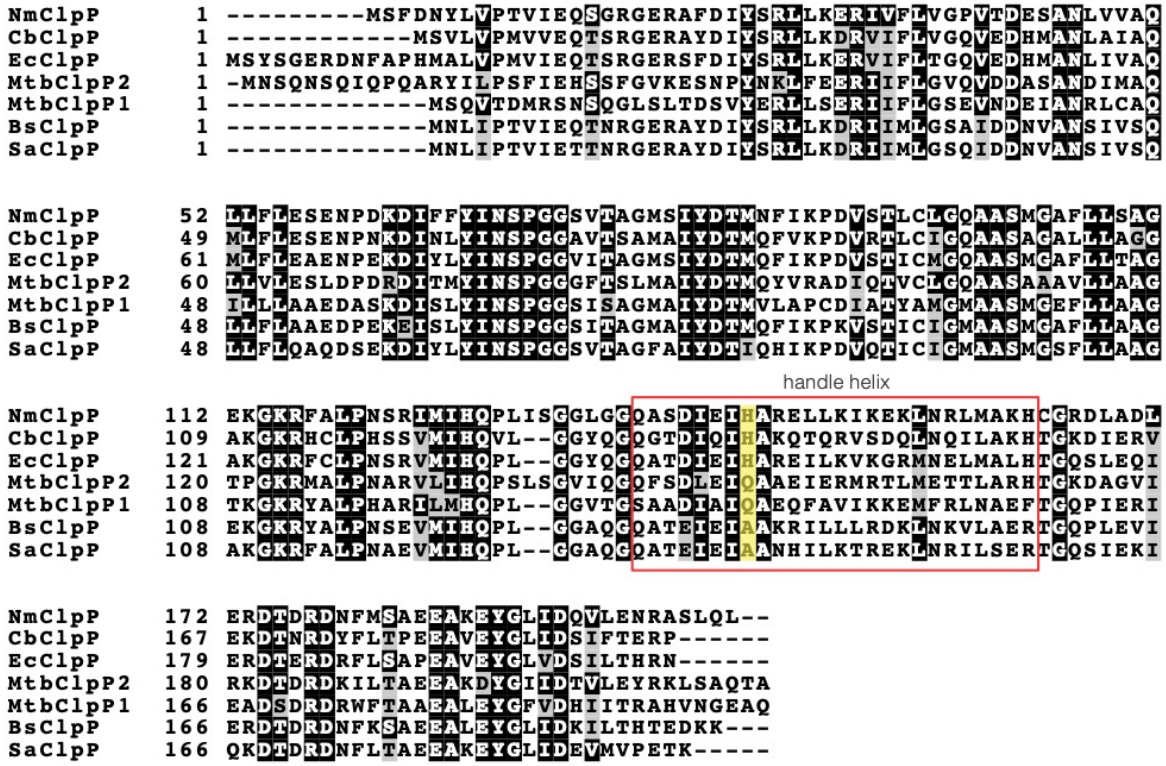

Figure S1. Multiple alignments of ClpP sequences from selected organisms, as indicated. The handle helix is highlighted in red, and the NmClpP H145 position is highlighted in yellow. The Uniprot identifiers for the sequences shown are (NmClpP) *Neisseria meningitidis* ClpP Q9JZ38; (CbClpP) *Coxiella burnetiid* ClpP B6J0W0; (EcClpP) *Escherichia coli* ClpP P0A6G7; (MtClpP1) *Mycobacterium tuberculosis* ClpP1 P9WPC5; (MtClpP2) *Mycobacterium tuberculosis* ClpP2 P9WPC3; (BsClpP) *Bacillus subtilis* ClpP P80244; (SaClpP) *Staphylococcus aureus* ClpP Q2G036.

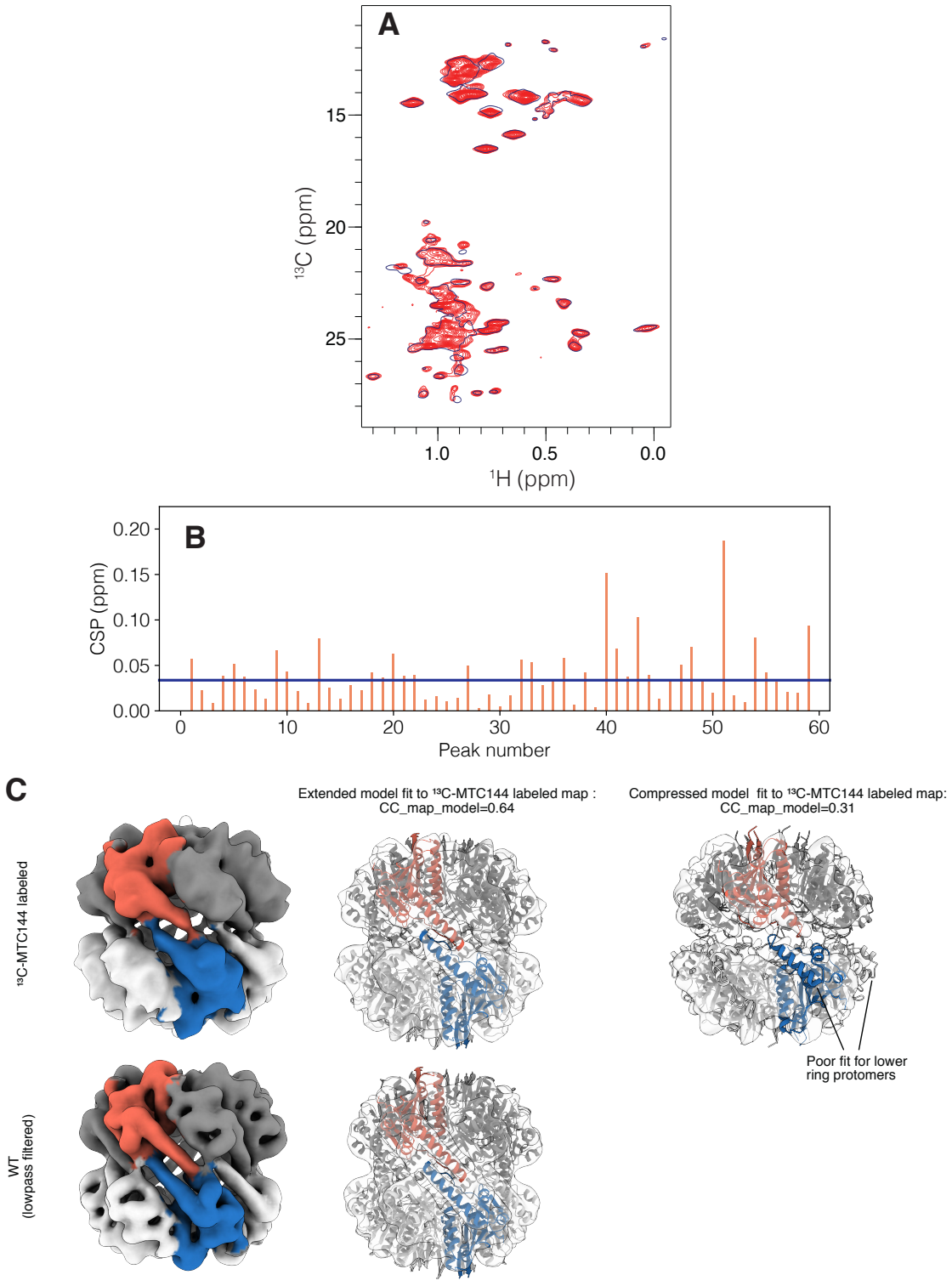

Figure S2. Wild-type (WT) and ^{13}C-MTC144 NmClpP are structurally similar. (A) Overlay of the Ile and Leu/Val regions of ^{1}H-^{13}C correlation maps of ILVM-labeled WT (single-contour,

blue) and ILVM-labeled, ^{13}C-MTC144 (multi-contour, red) NmClpP, pH 7.6, 40 ˚C, 18.8 T. The high degree of similarity between the HMQC spectra indicate that the introduction of the MTC moiety does not lead to significant structural perturbations (see discussion above). (B) ILVM methyl chemical shift perturbations (CSPs) between spectra of ILVM-labeled WT and ^{13}C-MTC144 NmClpP (panel A), calculated as $\Delta\delta = [(\Delta\delta_H/\alpha)^2+(\Delta\delta_C/\beta)^2]^{0.5}$, where $\Delta\delta_H$ and $\Delta\delta_C$ are chemical shift differences in the ^{1}H and ^{13}C dimensions (ppm), and α and β are the standard deviations of ^{1}H and ^{13}C chemical shift distributions deposited in the Biological Magnetic Resonance Data Bank (α=0.282, β=1.646 for Ile; α=0.266, β=1.470 for Leu/Val; α=0.387, β=1.736 for Met). The horizontal line corresponds to the median CSP = 0.034 ppm; (C) Cryo-EM analysis of ^{13}C-MTC144 NmClpP shows no discernible changes with respect to WT NmClpP. (top) Density map of MTC144 NmClpP (left) and a comparison of fits of the extended and compressed models into the MTC144 NmClpP map (right, pH 8.5). The MTC144 NmClpP map is much more consistent with the active extended form of ClpP than with a compressed conformation. Assuming that the addition of the MMTS label does not introduce structural perturbations this is to be expected because the sample was at pH 8.5 where the unlabeled enzyme is in the extended conformation. Thus, the MMTS label did not introduce significant changes to the overall conformation of ClpP. Cross-correlations between map and model were calculated in *PHENIX*[25]. (bottom) A map of unlabeled NmClpP at pH 8.5 low-pass filtered to 7.5 Å, the same resolution as for MTC144 NmClpP, along with the extended model is shown for comparison (bottom).

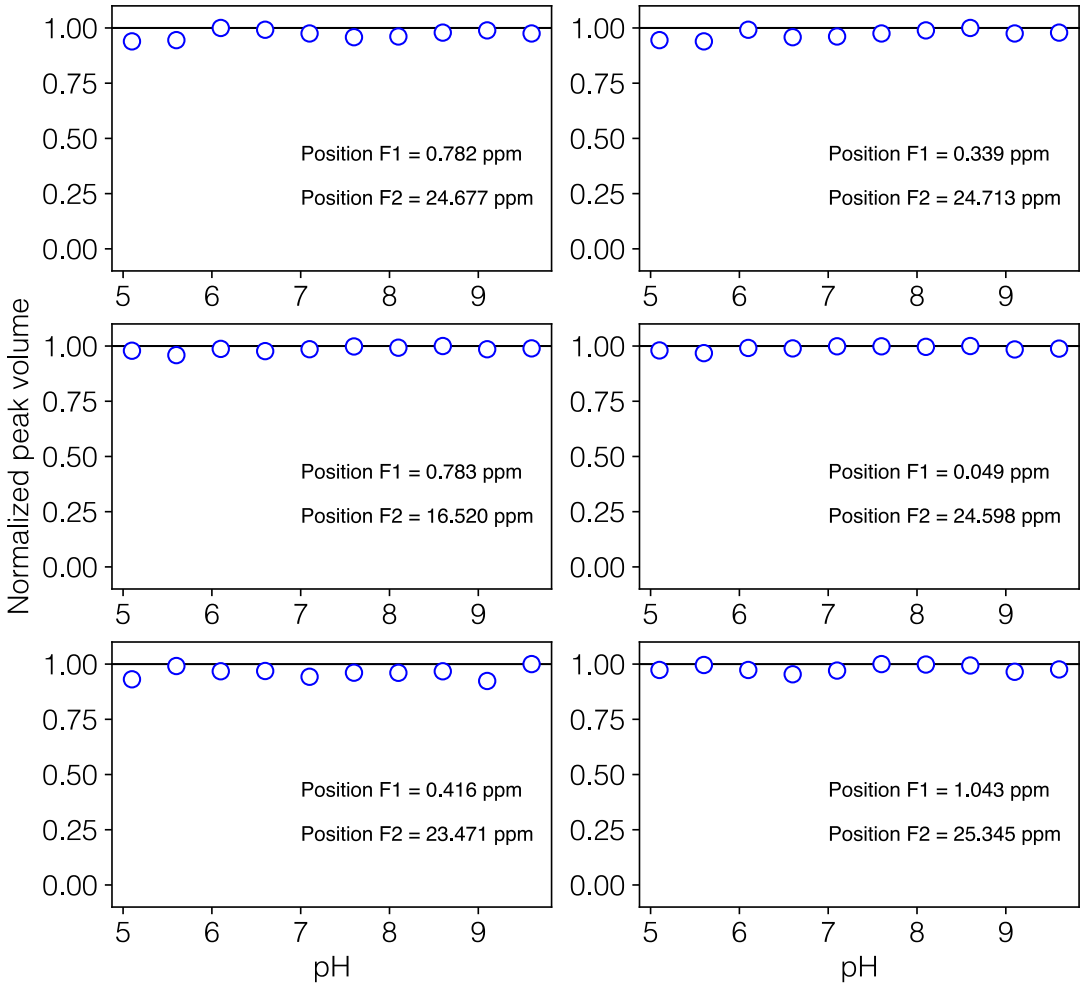

Figure S3. The majority of ILVM methyl resonances that could be easily quantified (75% of the 69 correlations in the HMQC spectrum) do not titrate with pH. Changes in the peak volumes of representative ILVM methyl resonances of ILVM-labeled ^{13}C-MTC144 NmClpP as a function of pH at 40 ˚C, 18.8 T. The chemical shift of each peak is indicated on the plots.

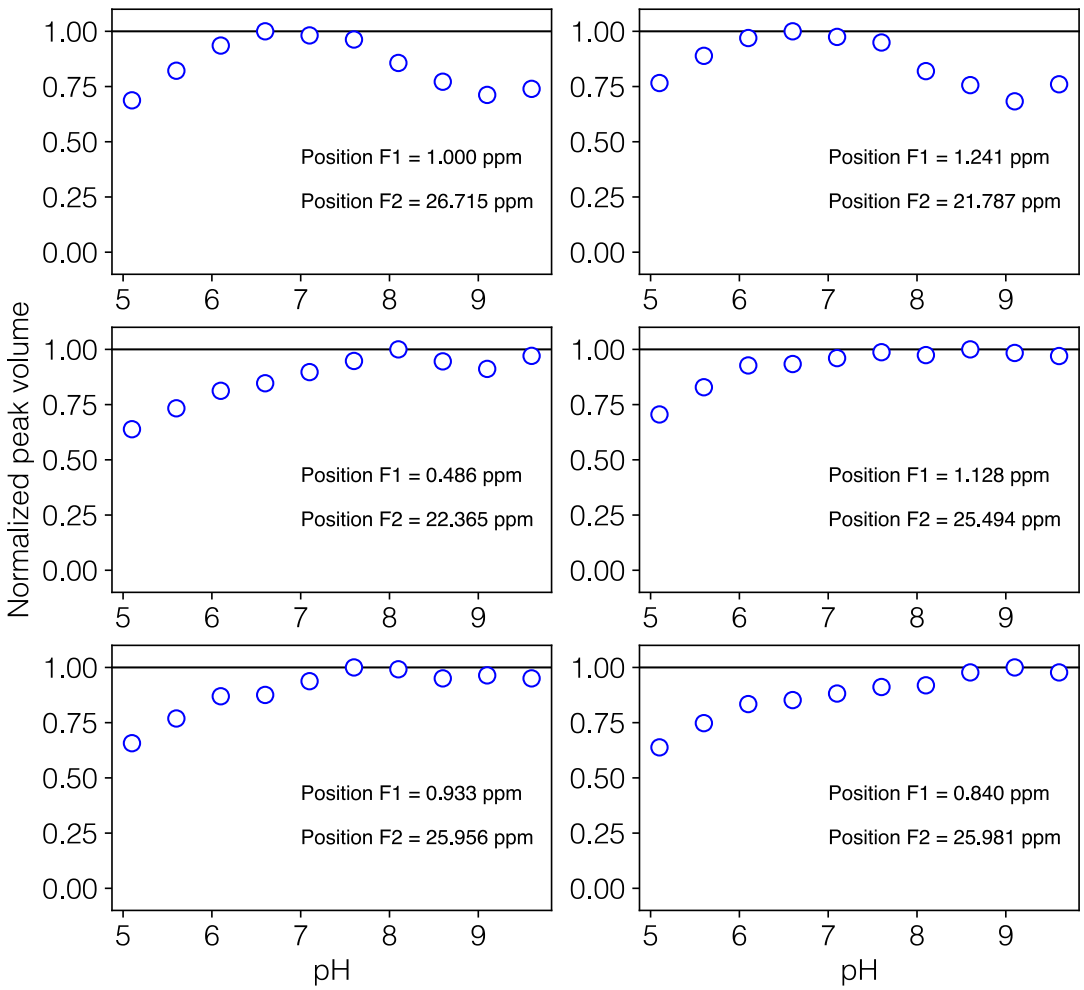

Figure S4. Peak volumes of a number of resonances change as a function of pH (approximately 25% of the 69 quantified correlations). None of these report the conformational transition observed via cryo-EM, and likely reflect changes in conformational exchange dynamics with pH. Peak volumes were extracted from ^{1}H-^{13}C HMQC maps of ILVM-labeled ^{13}C-MTC144 NmClpP as a function of pH at 40 ˚C, 18.8 T. The chemical shift of each peak is indicated on each plot.

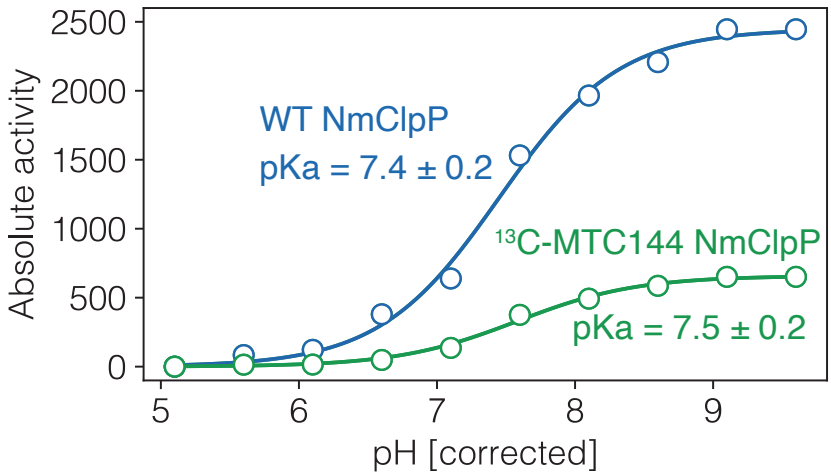

Figure S5. Peptidase activity assays of wild-type (blue circles) and ^{13}C-MTC144 NmClpP (green circles) performed as a function of pH with 250 µM PKM-AMC as substrate. Identical sample conditions were used in both cases, including deuteration levels of proteins. The activity profiles were fitted independently to a simple Henderson-Hasselbalch model assuming a single pK_a value (solid lines), with pK_a values of 7.4 ± 0.2 (wild-type) and 7.5 ± 0.2 (^{13}C-MTC144) obtained, indicating that the introduction of the MTC probe does not perturb the pH sensitivity of the system, and, further, that the structural perturbations introduced by the probe are minimal.

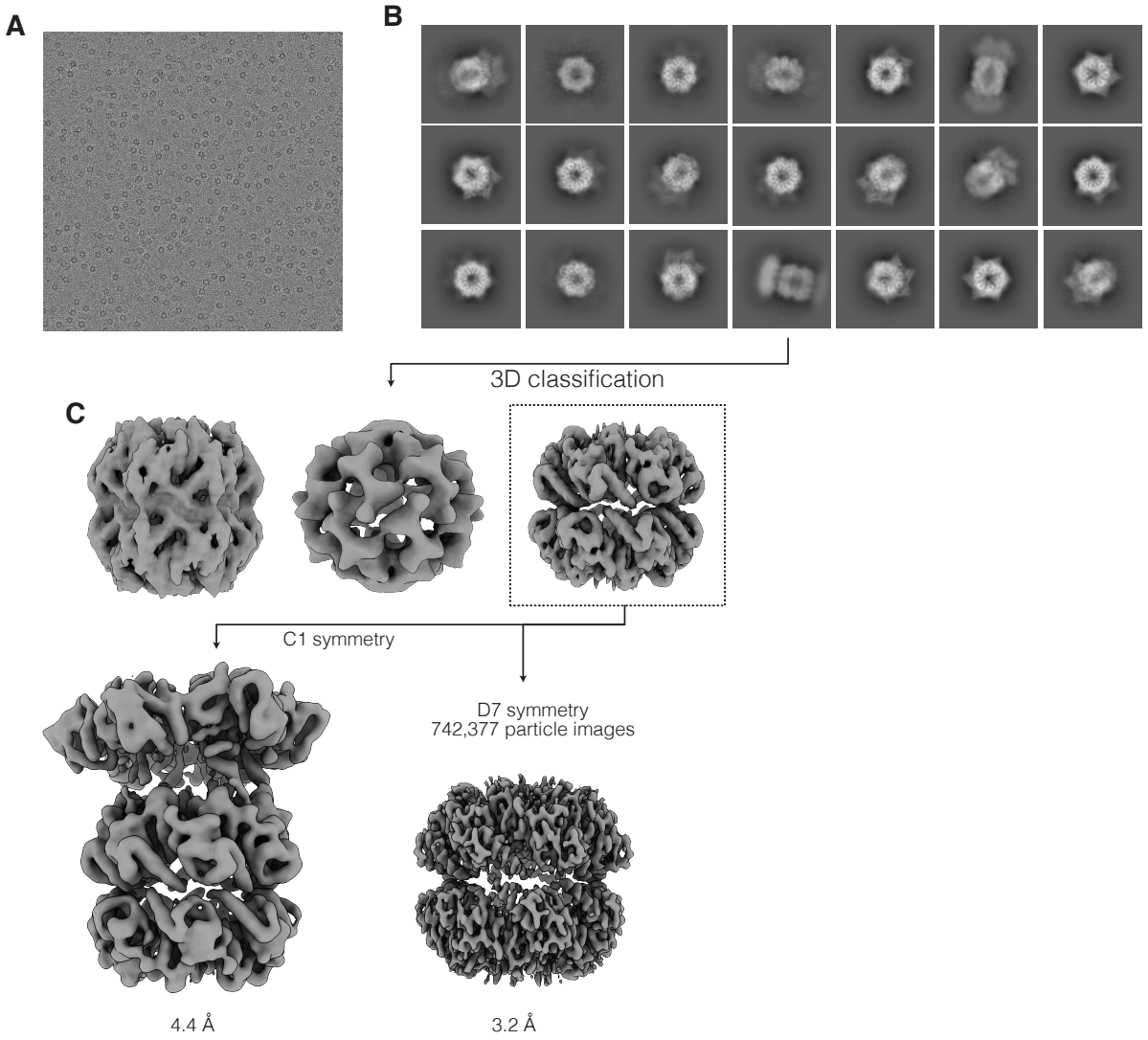

Figure S6. Cryo-EM processing pipeline. (A) Representative micrograph of NmClpXP at pH 7.0. (B) Subset of the selected 2D class averages that were carried forward into (C) 3D classification/heterogenous refinement with D7 symmetry. (D) The best class was then refined with either C1 or D7 symmetry, yielding a lower resolution ClpXP complex with poor resolution for both ClpX and ClpP (left), or a high-resolution reconstruction with strong density only for ClpP (right). Note that while the ClpXP complex is doubly capped (as evident in the 2D class averages) only a single ClpX appears in the C1 reconstruction, as the second ClpX is averaged over many positions, leading to much weaker density.

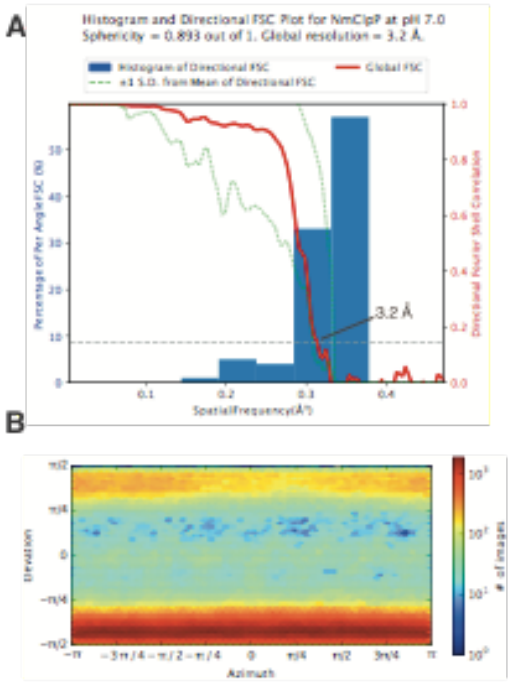

Figure S7. Resolution estimates for Cryo-EM reconstruction of NmClpP from the ClpXP complex at pH 7.0. (A) Histogram of directional Fourier shell correlation (FSC) plots, generated from 3D FSCs as implemented on the Remote 3DFSC Processing Server[21]. (B) Angular distribution of image poses used in final reconstruction.

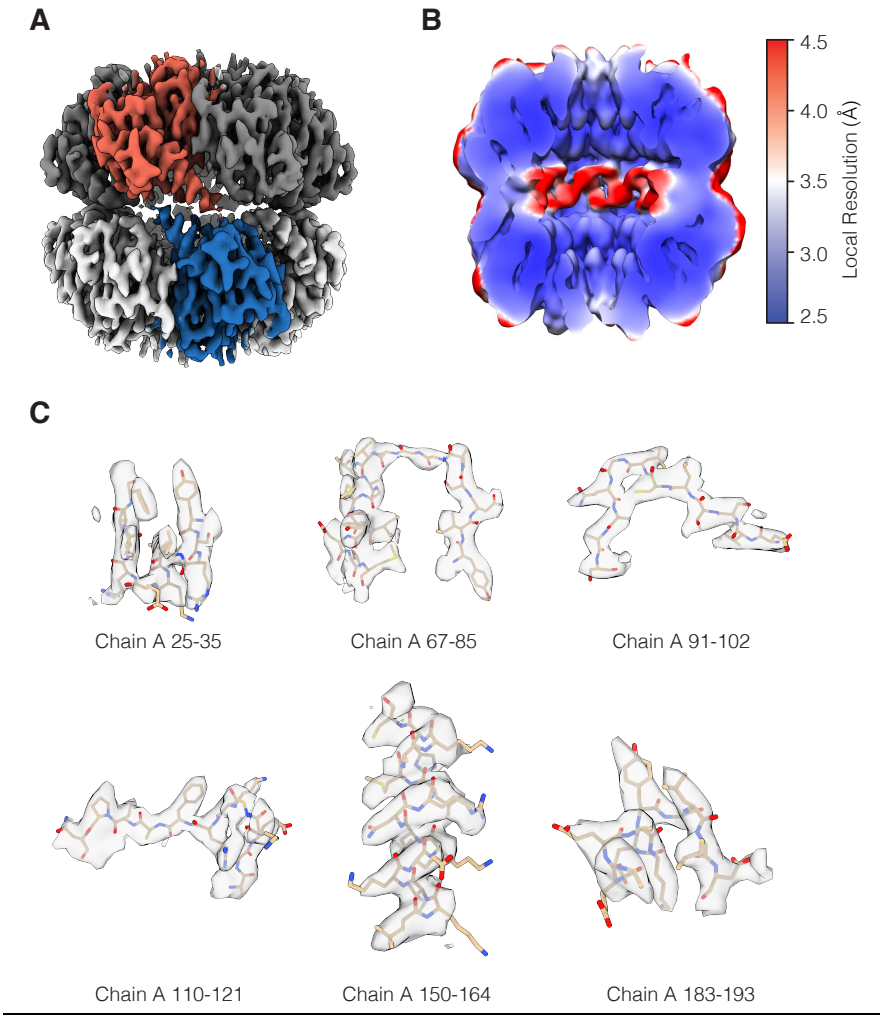

Figure S8. Cryo-EM of WT NmClpXP at pH 7.0. (A) Cryo-EM density map of the ClpP portion of the NmClpXP complex at pH 7.0. Single protomers in each ring are highlighted in red and blue. (B) Local resolution estimates for NmClpP; the density for the handle-sheet region (residues 131-142) appears at lower resolution than the rest of the complex, likely due to flexibility of the "sheet" which is not formed in the pH=7, inactive state. The density shown is unsharpened in order to emphasize the difference between the handle-sheet and the rest of the complex. (C) Model-in map fits for various regions of NmClpP at pH 7.0.

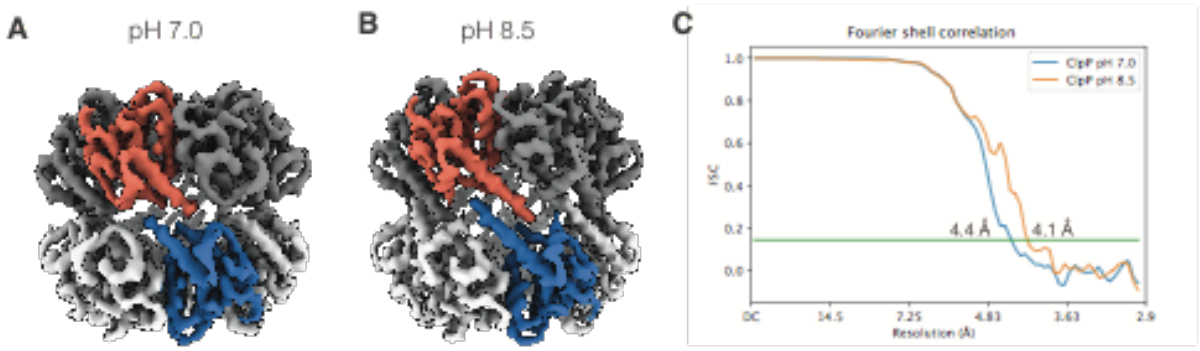

Figure S9. Cryo-EM density maps for isolated NmClpP at (A) pH 7.0 and (B) pH 8.5. (C) Fourier shell correlation curves for the two reconstructions.

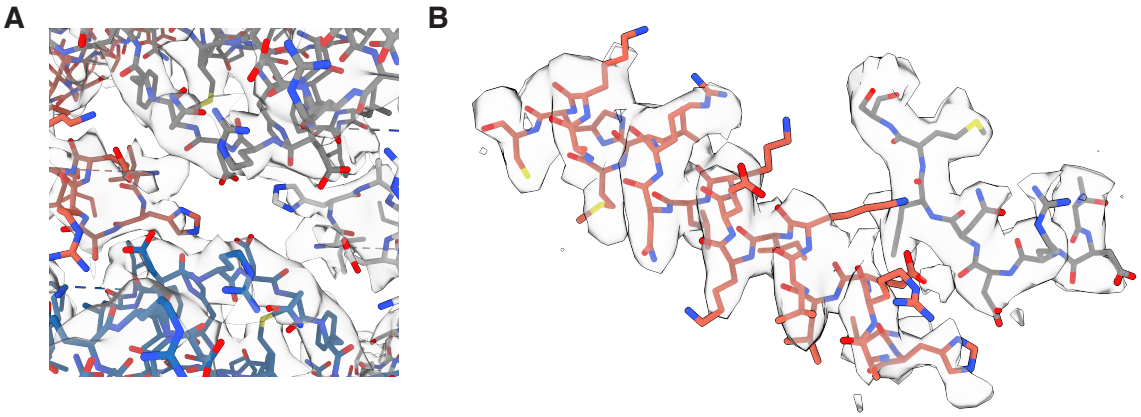

Figure S10. Model in map fits for the handle region of NmClp at pH 7.0. (A) The model and cryoEM density map is shown for the oligomeric sensor region. (B) Handle helix (pink) and oligomeric sensor (grey) are shown.

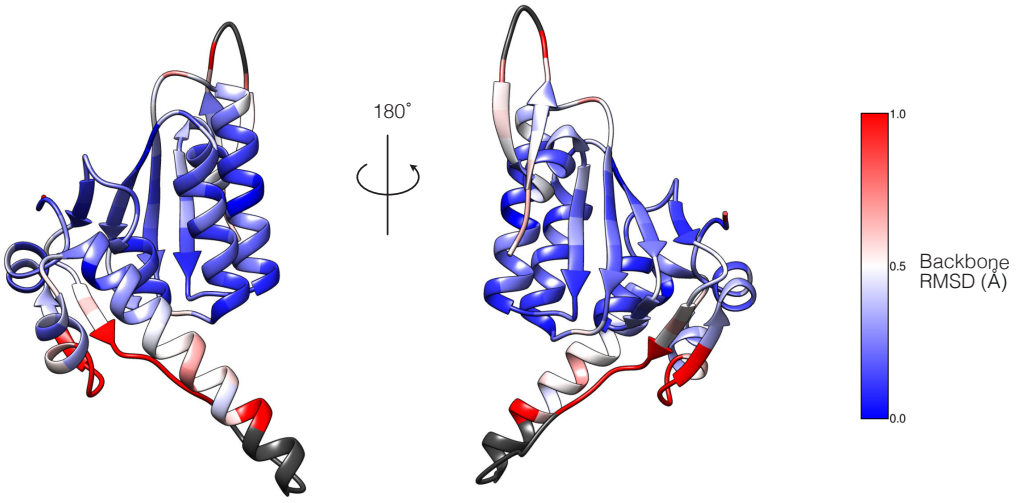

Figure S11. Backbone root-mean-square deviation (RMSD) (see legend) calculated between the active extended and inactive compressed conformations of NmClpP and mapped onto a single protomer of the extended form. Residues missing from the compressed model are excluded from this analysis and displayed in black.

Reference:

(1) Ripstein, Z. A.; Vahidi, S.; Houry, W. A.; Rubinstein, J. L.; Kay, L. E. A Processive Rotary Mechanism Couples Substrate Unfolding and Proteolysis in the ClpXP Degradation Machinery. *Elife* **2020**, *9*, e52158. https://doi.org/10.7554/eLife.52158.

(2) Tugarinov, V.; Kay, L. E. An Isotope Labeling Strategy for Methyl TROSY Spectroscopy. *J. Biomol. NMR* **2004**, *28* (2), 165–172. https://doi.org/10.1023/B:JNMR.0000013824.93994.1f.

(3) Tugarinov, V.; Hwang, P. M.; Ollerenshaw, J. E.; Kay, L. E. Cross-Correlated Relaxation Enhanced 1H−13C NMR Spectroscopy of Methyl Groups in Very High Molecular Weight Proteins and Protein Complexes. *J. Am. Chem. Soc.* **2003**, *125* (34), 10420–10428. https://doi.org/10.1021/ja030153x.

(4) Delaglio, F.; Grzesiek, S.; Vuister, G. W.; Zhu, G.; Pfeifer, J.; Bax, A. NMRPipe: A Multidimensional Spectral Processing System Based on UNIX Pipes. *J. Biomol. NMR* **1995**, *6* (3), 277–293. https://doi.org/10.1007/bf00197809.

(5) Vranken, W. F.; Boucher, W.; Stevens, T. J.; Fogh, R. H.; Pajon, A.; Llinas, M.; Ulrich, E. L.; Markley, J. L.; Ionides, J.; Laue, E. D. The CCPN Data Model for NMR Spectroscopy: Development of a Software Pipeline. *Proteins* **2005**, *59* (4), 687–696. https://doi.org/10.1002/prot.20449.

(6) Liu, K.; Ologbenla, A.; Houry, W. A. Dynamics of the ClpP Serine Protease: A Model for Self-Compartmentalized Proteases. *Crit. Rev. Biochem. Mol. Biol.* **2014**, *49* (5), 400–412. https://doi.org/10.3109/10409238.2014.925421.

(7) Vahidi, S.; Ripstein, Z. A.; Bonomi, M.; Yuwen, T.; Mabanglo, M. F.; Juravsky, J. B.; Rizzolo, K.; Velyvis, A.; Houry, W. A.; Vendruscolo, M.; Rubinstein, J. L.; Kay, L. E. Reversible Inhibition of the ClpP Protease via an N-Terminal Conformational Switch. *Proc. Natl. Acad. Sci. U.S.A.* **2018**, *115* (28), E6447–E6456. https://doi.org/10.1073/pnas.1805125115.

(8) Vahidi, S.; Ripstein, Z. A.; Juravsky, J. B.; Rennella, E.; Goldberg, A. L.; Mittermaier, A. K.; Rubinstein, J. L.; Kay, L. E. An Allosteric Switch Regulates Mycobacterium Tuberculosis ClpP1P2 Protease Function as Established by Cryo-EM and Methyl-TROSY NMR. *Proc. Natl. Acad. Sci. U. S. A.* **2020**, *117* (11), 5895–5906. https://doi.org/10.1073/pnas.1921630117.

(9) Felix, J.; Weinhäupl, K.; Chipot, C.; Dehez, F.; Hessel, A.; Gauto, D. F.; Morlot, C.; Abian, O.; Gutsche, I.; Velazquez-Campoy, A.; Schanda, P.; Fraga, H. Mechanism of the Allosteric Activation of the ClpP Protease Machinery by Substrates and Active-Site

Inhibitors. *Sci. Adv.* **2019**, *5* (9), eaaw3818. https://doi.org/10.1126/sciadv.aaw3818.

(10) Gersch, M.; Famulla, K.; Dahmen, M.; Göbl, C.; Malik, I.; Richter, K.; Korotkov, V. S.; Sass, P.; Rübsamen-Schaeff, H.; Madl, T.; Brötz-Oesterhelt, H.; Sieber, S. A. AAA+ Chaperones and Acyldepsipeptides Activate the ClpP Protease via Conformational Control. *Nat. Commun.* **2015**, *6*, 6320. https://doi.org/10.1038/ncomms7320.

(11) Geiger, S. R.; Bottcher, T.; Sieber, S. A.; Cramer, P. A Conformational Switch Underlies ClpP Protease Function. *Angew.Chem.Int.Ed.Engl.* **2011**, *50*, 5749–5752. https://doi.org/10.2210/PDB3QWD/PDB.

(12) Vahidi, S.; Ripstein, Z. A.; Juravsky, J. B.; Rennella, E.; Goldberg, A. L.; Mittermaier, A. K.; Rubinstein, J. L.; Kay, L. E. An Allosteric Switch Regulates Mycobacterium Tuberculosis ClpP1P2 Protease Function as Established by Cryo-EM and Methyl-TROSY NMR. *Proc. Natl. Acad. Sci.* **2020**. https://doi.org/10.1073/pnas.1921630117.

(13) Religa, T. L.; Ruschak, A. M.; Rosenzweig, R.; Kay, L. E. Site-Directed Methyl Group Labeling as an NMR Probe of Structure and Dynamics in Supramolecular Protein Systems: Applications to the Proteasome and to the CIpP Protease. *J. Am. Chem. Soc.* **2011**, *133* (23), 9063–9068. https://doi.org/10.1021/ja202259a.

(14) Huang, R.; Ripstein, Z. A.; Augustyniak, R.; Lazniewski, M.; Ginalski, K.; Kay, L. E.; Rubinstein, J. L. Unfolding the Mechanism of the AAA+ Unfoldase VAT by a Combined Cryo-EM, Solution NMR Study. *Proc. Natl. Acad. Sci. U.S.A.* **2016**, *113* (29), E4190–E4199. https://doi.org/10.1073/pnas.1603980113.

(15) Farmer, B. T.; Constantine, K. L.; Goldfarb, V.; Friedrichs, M. S.; Wittekind, M.; Yanchunas, J.; Robertson, J. G.; Mueller, L. Localizing the NADP+ Binding Site on the MurB Enzyme by NMR. *Nat. Struct. Biol.* **1996**, *3* (12), 995–997.

https://doi.org/10.1038/nsb1296-995.

(16) Newville, M.; Stensitzki, T.; Allen, D. B.; Ingargiola, A. LMFIT: Non-Linear Least-Square Minimization and Curve-Fitting for Python. Zenodo September 2014. https://doi.org/10.5281/zenodo.11813.

(17) Frolkovič, P. Numerical Recipes: The Art of Scientific Computing. *Acta Appl. Math.* **1990**, *19* (3), 297–299. https://doi.org/10.1007/BF01321860.

(18) Marr, C. R.; Benlekbir, S.; Rubinstein, J. L. Fabrication of Carbon Films with Approximately 500 Nm Holes for Cryo-EM with a Direct Detector Device. *J Struct Biol* **2014**, *185* (1), 42–47. https://doi.org/10.1016/j.jsb.2013.11.002.

(19) Tivol, W. F.; Briegel, A.; Jensen, G. J. An Improved Cryogen for Plunge Freezing. *Microsc. Microanal.* **2008**, *14* (5), 375–379. https://doi.org/10.1017/S1431927608080781.

(20) Punjani, A.; Rubinstein, J. L.; Fleet, D. J.; Brubaker, M. a. CryoSPARC: Algorithms for Rapid Unsupervised Cryo-EM Structure Determination. *Nat. Methods* **2017**, *14* (2), 290–296. https://doi.org/10.1038/nmeth.4169.

(21) Zi Tan, Y.; Baldwin, P. R.; Davis, J. H.; Williamson, J. R.; Potter, C. S.; Carragher, B.; Lyumkis, D. Addressing Preferred Specimen Orientation in Single-Particle Cryo-EMthrough Tilting. *Nat. Methods* **2017**, *14* (8), 793–796. https://doi.org/10.1038/nmeth.4347.

(22) Pettersen, E. F.; Goddard, T. D.; Huang, C. C.; Couch, G. S.; Greenblatt, D. M.; Meng, E. C.; Ferrin, T. E. UCSF Chimera—A Visualization System for Exploratory Research and Analysis. *J. Comp. Chem.* **2004**, *25* (13), 1605–1612. https://doi.org/10.1002/jcc.20084.

(23) Emsley, P.; Cowtan, K. Coot: Model-Building Tools for Molecular Graphics. *Acta Crystallogr. Sect. D* **2004**, *60* (12 Part 1), 2126–2132.

https://doi.org/10.1107/S0907444904019158.

(24) Wang, R. Y.-R.; Song, Y.; Barad, B. A.; Cheng, Y.; Fraser, J. S.; DiMaio, F. Automated Structure Refinement of Macromolecular Assemblies from Cryo-EM Maps Using Rosetta. *Elife* **2016**, *5*, e17219. https://doi.org/10.7554/eLife.17219.

(25) Adams, P. D.; Afonine, P. V; Bunkóczi, G.; Chen, V. B.; Davis, I. W.; Echols, N.; Headd, J. J.; Hung, L.-W.; Kapral, G. J.; Grosse-Kunstleve, R. W.; McCoy, A. J.; Moriarty, N. W.; Oeffner, R.; Read, R. J.; Richardson, D. C.; Richardson, J. S.; Terwilliger, T. C.; Zwart, P. H. PHENIX: A Comprehensive Python-Based System for Macromolecular Structure Solution. *Acta Crystallogr. Sect. D* **2010**, *66* (2), 213–221. https://doi.org/10.1107/S0907444909052925.

(26) Barad, B. A.; Echols, N.; Wang, R. Y.-R.; Cheng, Y.; DiMaio, F.; Adams, P. D.; Fraser, J. S. EMRinger: Side Chain–Directed Model and Map Validation for 3D Cryo-Electron Microscopy. *Nat. Methods* **2015**, *12*, 943.

(27) Goddard, T. D.; Huang, C. C.; Meng, E. C.; Pettersen, E. F.; Couch, G. S.; Morris, J. H.; Ferrin, T. E. UCSF ChimeraX: Meeting Modern Challenges in Visualization and Analysis. *Protein Sci.* **2018**, *27* (1), 14–25. https://doi.org/10.1002/pro.3235.